Materials Research Express

PAPER • **OPEN ACCESS**

Improved performance of perovskite photodetectors with a hybrid planar-mixed heterojunction

To cite this article: Hairuo Wu *et al* 2020 *Mater. Res. Express* **7** 066201

Materials Research Express

PAPER

Improved performance of perovskite photodetectors with a hybrid planar-mixed heterojunction

Hairuo Wu[1,2], **Bei Chu**[1,4] **and Zisheng Su**[3,4]

[1] State Key Laboratory of Luminescence and Applications, Changchun Institute of Optics, Fine Mechanics and Physics, Chinese Academy of Sciences, Changchun 130033, People's Republic of China
[2] University of Chinese Academy of Sciences, Beijing 100039, People's Republic of China
[3] College of Physics and Information Engineering, Key Laboratory of Information Functional Material for Fujian Higher Education and Fujian Key Laboratory for Advanced Micro-Nano Photonics Technology and Devices, Quanzhou Normal University, Quanzhou 362000, People's Republic of China
[4] Authors to whom any correspondence should be addressed.

E-mail: chub@ciomp.ac.cn **and** suzs@ciomp.ac.cn

Keywords: perovskite photodetector, heterojunction, grain boundary, electron transfer

Supplementary material for this article is available online

OPEN ACCESS

RECEIVED
14 April 2020

REVISED
17 May 2020

ACCEPTED FOR PUBLICATION
2 June 2020

PUBLISHED
10 June 2020

Abstract

Improved performance of lateral perovskite photodetectors is demonstrated based on a hybrid planar-mixed heterojunction structure, which comprises a $CH_3NH_3PbI_3$:$PC_{61}BM$ ([6,6]-phenyl-C61-butyric acid methyl ester) bulk heterojunction on a planar SnO_2 layer. The photodetector with an optimized $PC_{61}BM$ doping concentration shows a photocurrent more than three times to that device without a $PC_{61}BM$ doping or without a planar SnO_2 layer, confirming that the hybrid planar-mixed heterojunction structure plays an important role in improving the performance of the devices. The photodetector exhibits a responsivity higher than 2 A W^{-1} in a wide range from ultraviolet to near infrared with a maximum one of 9 A W^{-1} at 315 nm. The improved performance is not only attributed to the increased electron transporting ability and the dissociation probability of excitons and/or electron-hole pairs in perovskite, but also to the growth of compact perovskite films with decreased grain boundary and hence the increased charge carriers transporting efficiency due to the introduction of $PC_{61}BM$.

1. Introduction

Organic/inorganic hybrid perovskites have emerged as the active materials for many optoelectronic devices, such as solar cells and light-emitting diodes, due to their merits of direct bandgap, large absorption coefficient, high carrier mobility, long exciton diffusion length, and compatible with various substrates [1–6]. Perovskite photodetectors, which have the potential applications in optical communications, environmental monitors, imaging, and chemical/biological sensing, have also attracted more and more attention since the first device demonstrated in 2014 [7–14]. From the structure point of view, there are typically two types perovskite photodetectors, e.g., vertical- and lateral-type devices. Compared with the vertical counterparts, the lateral photodetectors are easy to obtain a photocurrent gain because of the photoconduction working mechanism of these devices. Many strategies have been proposed to improve the performance of these photodetectors, one of which is to adopt a planar heterojunction structure. The materials that can be combined with perovskites to form such a planar heterojunction including two dimensional materials, organic, and inorganic semiconductors [15–21]. Similarly, a bulk heterojunction structure is also exploited [22–25]. Among the materials used in such a bulk heterojunciton, [6,6]-phenyl-C61-butyric acid methyl ester ($PC_{61}BM$) has gained the most attention [26–30]. On one hand, $PC_{61}BM$ can act as an electron acceptor that increases the dissociation efficiency of the photogenerated excitons or electron-hole pairs in the perovskites. On the other hand, it can passive the defect states in the perovskite grain boundary and increase the conductivity of the film, which compensates the lower diffusion length of electron compared to the hole one in the perovskite films [31–34].

In previous work, we have demonstrated that the performance of the perovskite photodetector can be improved with a $CH_3NH_3PbI_3/SnO_2$ planar heterojunction [35]. In this work, a hybrid planar-mixed hetrojunction is adopted to further improve their performance. The hybrid planar-mixed hetrojunction perovskite photodetectors comprise a $CH_3NH_3PbI_3$:$PC_{61}BM$ bulk heterojunction on a planar SnO_2 layer. The photodetector with an optimized $PC_{61}BM$ doping concentration shows a photocurrent more than three times to that device without a $PC_{61}BM$ doping or without a planar SnO_2 layer. Correspondingly, the optimized device exhibits a responsivity higher than 2 A W^{-1} in a wide range from ultraviolet to near infrared with a maximum one of 9 A W^{-1} at 315 nm. This work confirms that the hybrid planar-mixed heterojunction structure is effect in improving the performance of the lateral perovskite photodetectors.

2. Experimental details

The $CH_3NH_3PbI_3$ precursor solution was prepared by dissolving CH_3NH_3I and PbI_2 at 1:1 (0.162:0.462 g) equimolar ratio in 0.7 ml N,N-dimethylformamid and 0.3 ml dimethyl sulfoxide, and the solution was stirred for 12 hours at 70 °C before using. For the bulk heterojunction films, 0.05, 0.1, and 0.5 mg $PC_{61}BM$ were added to the $CH_3NH_3PbI_3$ precursor solution, respectively, which formed different doping concentration of $PC_{61}BM$ in $CH_3NH_3PbI_3$ films. The photodetectors were fabricated on ultraviolet-ozone treated glass substrates. Firstly, SnO_2 aqueous solution was spin-coated onto the pretreated glass substrates at a rate of 3000 rpm and then annealed at 150 °C for 30 min, which formed a SnO_2 layer of about 140 nm [35]. $CH_3NH_3PbI_3$:$PC_{61}BM$ bulk heterojunction films were then spin-coated on the SnO_2 layer from the $CH_3NH_3PbI_3$ precursor solution with a rate of 500 rpm for 5 s and 3000 rpm for 60 s in sequence. After 20 s delay, 300 μl chlorobenzene was quickly added during the spin-coating procedure. The substrates were then annealed at 70 and 105 °C for 3 and 10 min, respectively. All the above processes were carried out in ambient conditions. Au electrodes were thermally deposited onto the $CH_3NH_3PbI_3$:$PC_{61}BM$ films with a rate of 2 Å s^{-1} in a vacuum chamber at a pressure of $\sim 5 \times 10^{-4}$ Pa through a shadow mask, defining the channel length and width of 1000 and 60 μm, respectively. The morphologies of the films were obtained on a Hitachi S4800 scanning electron microscopy (SEM). X-ray diffraction (XRD) pattern was measured with a Rigaku D/Max-2500 x-ray diffractometer using a Cu Kα radiation ($\lambda = 1.540\,56$ Å). Absorption spectra were recorded on a Shimadzu UV-3101PC spectrophotometer. The current-voltage (I-V) characteristics were measured using a Keithley 2400 sourcemeter. The external quantum efficiency (EQE) data was measured with a Stanford SR803 lock-in amplifier under monochromatic illumination at a chopping frequency of 130 Hz by a Stanford SR540 chopper, and the monochromatic lights were obtained from a monochromater under illumination of a 300 mW cm^{-2} Xenon lamp. All measurements were performed under ambient conditions and at room temperature.

3. Results and discussion

The surface morphology of the $CH_3NH_3PbI_3$:$PC_{61}BM$ films on SnO_2 are shown in figure 1. From the SEM images with a lower amplification ratio (upper in figure 1), it can be found that there are some pin holes in the pristine $CH_3NH_3PbI_3$ film. The size of the pin holes decreases but the density increases in the 0.05 mg ml^{-1} $PC_{61}BM$ doped $CH_3NH_3PbI_3$ film. Further increase the concentration of $PC_{61}BM$ results in decreases of both the size and density of the pin holes. From the SEM images with a larger amplification ratio (lower in figure 1), it can be found that the average grain size in the pristine $CH_3NH_3PbI_3$ film is about 300 nm. However, the average grain size in the 0.05 mg ml^{-1} $PC_{61}BM$ doped $CH_3NH_3PbI_3$ film is a little lower, but it increases with the doping concentration of $PC_{61}BM$ and a size of about 300 nm in found in the 0.5 mg ml^{-1} $PC_{61}BM$ doped $CH_3NH_3PbI_3$ film. The compact morphology of the perovskite films doped with $PC_{61}BM$ decreases the grain boundary and hence the decreased defect state density and increased charge carrier transporting efficiency. Meanwhile, the $PC_{61}BM$ can also passive the defect states and increase the conductivity of the perovskite films [31–34]. These properties indicate that hybrid planar-mixed heterojunction structure may be favorable in improving the performance of the lateral perovskite photodetectors.

Figure 2 illuminates the XRD patterns of the $CH_3NH_3PbI_3$:$PC_{61}BM$ films on SnO_2. The XRD pattern of the pristine $CH_3NH_3PbI_3$ film presents obvious diffraction peaks at 14.26°, 28.34°, and 32.02°, which originates from the reflections of (110), (220), and (310) crystal planes of $CH_3NH_3PbI_3$, respectively [36]. Similar diffraction peaks are found in the $CH_3NH_3PbI_3$:$PC_{61}BM$ films. However, a small diffraction peak of PbI_2 at 12.7° is found in the 0.5 mg ml^{-1} $PC_{61}BM$ doped $CH_3NH_3PbI_3$ film, suggesting that the PbI_2 is not fully converted to $CH_3NH_3PbI_3$ when a high concentration of $PC_{61}BM$ is employed. This is attributed to the aggregation of $PC_{61}BM$ at a higher concentration, which disturbs the growth dynamic of the perovskite film.

Figure 3 displays the I–V characteristics of the photodetectors under illumination of an AM 1.5G solar simulator with an intensity of 100 mW cm^{-2}. The structure of the photodetector is shown in the inset of figure 4.

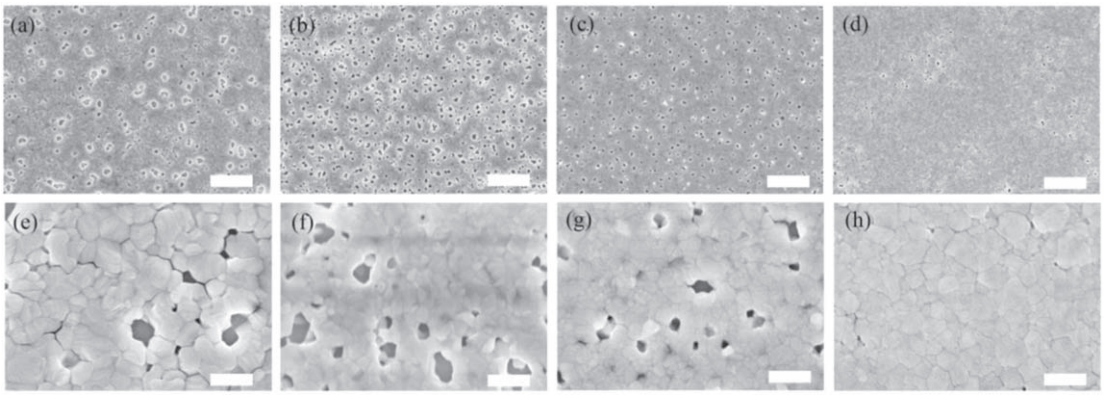

Figure 1. SEM image of the $CH_3NH_3PbI_3$:$PC_{61}BM$ films on SnO_2 with a $PC_{61}BM$ doping concentration of (a) 0, (b) 0.05, (c) 0.1, and (d) 0.5 mg ml^{-1}, (e)–(h) the corresponding films with a higher amplification ratio, and the scale bars in (a)–(d) are 2 μm and in (e)–(h) are 400 nm.

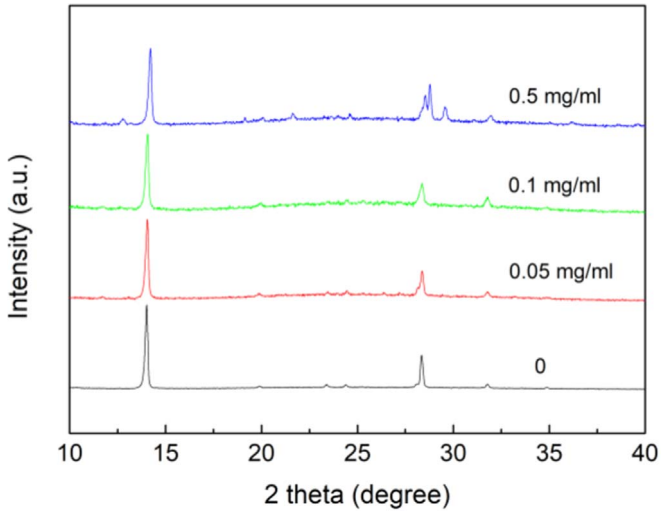

Figure 2. XRD patterns of the $CH_3NH_3PbI_3$:$PC_{61}BM$ films on SnO_2 with different $PC_{61}BM$ doping concentrations.

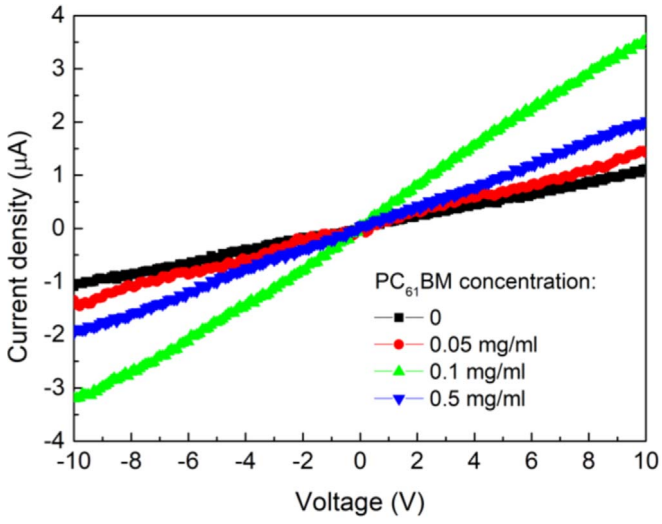

Figure 3. I–V characteristics of the photodetectors under illumination of an AM 1.5G solar simulator with an intensity of 100 mW cm^{-2}, inset: device structure of the hybrid planar-mixed heterojunction photodetectors.

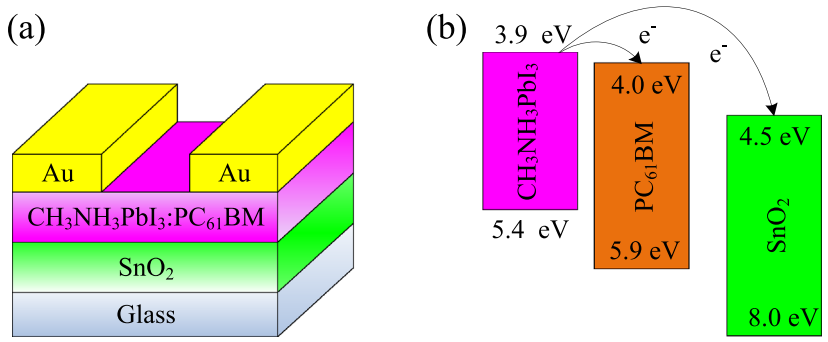

Figure 4. (a) Device structure of the hybrid planar-mixed heterojunction perovskite photodetectors, (b) schematic electron transfer in the photodetectors.

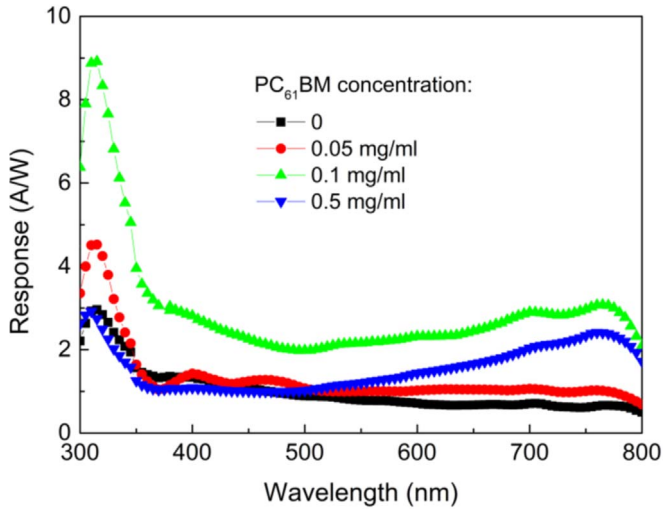

Figure 5. Responsivity of the hybrid planar-mixed heterojunction photodetectors at 1 V.

The $CH_3NH_3PbI_3$:$PC_{61}BM$ bulk heterojunction film on planar SnO_2 layer forms a hybrid planar-mixed heterojunction. All the photodetectors present a nearly linear I–V curves, suggesting an Ohmic contact between $CH_3NH_3PbI_3$ and Au electrodes. The photocurrent of the photodetector based on pristine $CH_3NH_3PbI_3$ is about 1.12 μA at 10 V. The photocurrent is dramatically increased for the photodetectors with $CH_3NH_3PbI_3$:$PC_{61}BM$ bulk heterojunction films. Among the photodetectors, the device with a 0.1 mg ml^{-1} $PC_{61}BM$ exhibits the highest photocurrent of 3.55 μA at 10 V, which is increased more than two times compared to the pristine CH_3NH_3PbI device. Besides, the dark current of the devices are all in the orders of 10^{-9} A, which provides an ON/OFF ratio in the orders of 10^3.

The responsivity of the photodetectors can be extracted from their EQE spectra. Figure 5 reveals the responsivity of the photodetectors at 1 V. A broad band response is found for all the devices. The similar shape of the response spectra suggests that the excitons of $PC_{61}BM$ contributes little to the photocurrent of the photodetectors, which may be attributed to its lower concentration. Among the photodetectors, the device with a 0.1 mg ml^{-1} $PC_{61}BM$ exhibits the highest responsivity in the whole response region, which is consistent to trend found in the I–V curves. Moreover, the responsivity is higher than 2 A W^{-1} in the whole response region, and a maximum one of about 9 A W^{-1} is obtained at 315 nm.

The response speed is another important figure-of-merit of a photodetector. Figure 6 shows the transient photocurrent of the optimized SnO_2/$CH_3NH_3PbI_3$:$PC_{61}BM$ photodetector at 1 V. The device was under illumination of a white light, and the light on and off were tuned by a SR540 optical chopper at a frequency of 12.5 Hz. The rise time is defined as the time for the photocurrent of the photodetector to reach 90% of its maximum value, while the decay time is for the photocurrent decreases to 10% of its maximum value. The rise and decay times of the optimized photodetector is about 10 and 8 ms, respectively. Such responses are comparable to our previous reported SnO_2/$CH_3NH_3PbI_3$ photodetector [35]. It should be noted that it needs a time for the chopper to open and block the light. However, this time is in the range of 0.1 to 0.2 ms that

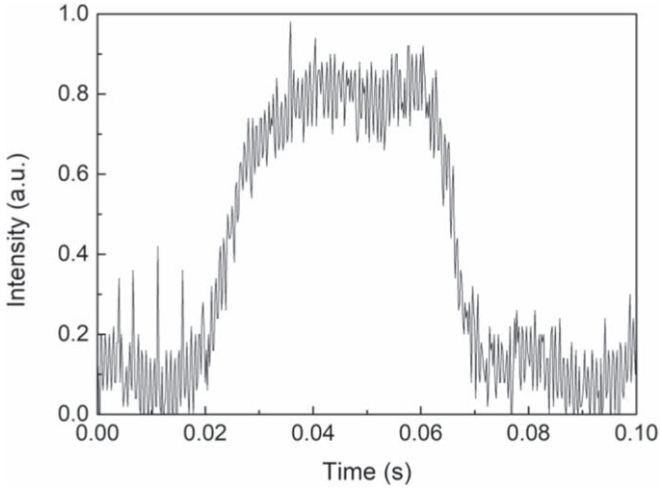

Figure 6. Response speed of the optimized $SnO_2/CH_3NH_3PbI_3$:$PC_{61}BM$ photodetector at 1 V.

calculated from the frequency of the optical chopper and of the size of the chopper blade. Comparing with the response times obtained from the transient photocurrent, such a time is significant shorter and can be ignored.

To understand the mechanisms for the improved performance of the hybrid planar-mixed heterojunction photodetectors, a photodetector with a 0.1 mg ml^{-1} $PC_{61}BM$ doped $CH_3NH_3PbI_3$ film on a glass substrate was also fabricated. Figure S1 is available online at stacks.iop.org/MRX/7/066201/mmedia shows the SEM images of the $CH_3NH_3PbI_3$:$PC_{61}BM$ film on glass substrate. A similar morphology with some pin-holes to that film on SnO_2 is found, which indicates that a limit contribution of the morphology to the improved performance of the photodetector. The XRD pattern shown in figure S2 reveals a small diffraction originated from PbI_2 at 12.7°, suggesting that small amount PbI_2 residual in the film. However, the photodetector based on this film shows a photocurrent of only 1 μA at 10 V under illumination of an AM 1.5G solar simulator with an intensity of 100 mW cm^{-2} (figure S3). To reveal the absorption on the performance of the photodetectors, the absorption spectra of the $CH_3NH_3PbI_3$:$PC_{61}BM$ films on glass and SnO_2 are investigated, as shown in figure S4. Both the two films appear an absorption edge of about 780 nm, corresponding to a band-gap of 1.59 eV of $CH_3NH_3PbI_3$. The similar absorption of these two films rules out that the increased photocurrent of the hybrid planar-mixed heterojunction device is raised from the increased absorption. It should be noted that the contribution of the absorption of SnO_2 on the total absorption of the device can be ignored although SnO_2 has an absorption band at ultraviolet region, which is attributed to its significant lower absorption (in the orders of 10^2) compared with $CH_3NH_3PbI_3$ as demonstrated in our previous work [35]. As a result, the mechanisms of the improved performance of the hybrid planar-mixed heterojunction photodetectors can be explained as follows. On one hand, the $PC_{61}BM$ in the hybrid planar-mixed heterojunction structure manipulates the growth of the $CH_3NH_3PbI_3$ films to form a more compact morphology with less grain boundary on SnO_2, which decreases the defect state density and increases the conductivity of the films. Besides, the $PC_{61}BM$ can also passive the defect states in the $CH_3NH_3PbI_3$ grain boundary, which reduces the recombination probability of the photogenerated charge carriers. On the other hand, the SnO_2 and $PC_{61}BM$ can also act as the electron acceptors for $CH_3NH_3PbI_3$. As shown in figure 4, the LUMO of $CH_3NH_3PbI_3$ is 3.9 eV, while they are 4.0 and 4.5 eV for $PC_{61}BM$ and SnO_2, respectively. Thus electrons in $CH_3NH_3PbI_3$ can be effectively transfer to $PC_{61}BM$ and SnO_2, which boost the dissociation efficiency of the excitons or electron-hole pairs formed in $CH_3NH_3PbI_3$ under illumination.

4. Conclusion

In conclusion, improved performance of the lateral perovskite photodetectors is demonstrated based on a hybrid planar-mixed heterojunction structure, which comprises a $CH_3NH_3PbI_3$:$PC_{61}BM$ bulk heterojunction on a planar SnO_2 layer. The photodetector with an optimized $PC_{61}BM$ doping concentration shows a responsivity of 9 A W^{-1}, which is more than three times to that device without a $PC_{61}BM$ doping or a planar SnO_2 layer. It is found that the introductions of $PC_{61}BM$ facilitates the growth of compact perovskite films and hence decreased the grain boundary, while the $PC_{61}BM$ also passive the defect states in the $CH_3NH_3PbI_3$ grain boundary. These effects increase the conductivity of the devices. On the other hand, the SnO_2 and $PC_{61}BM$ can act as the electron acceptors for $CH_3NH_3PbI_3$, which boosts the dissociation efficiency of the excitons or

electron-hole pairs formed in $CH_3NH_3PbI_3$ under illumination. These results confirm that the hybrid planar-mixed heterojunction structure plays an important role in improving the performance of the photodetectors. Such a structure may have potential applications in constructing high performance perovskite photodetectors.

Acknowledgments

This work was supported by the National Natural Science Foundation of China (61376062 and 61575192) and the Program for New Century Excellent Talents in Fujian Province University.

ORCID iDs

Zisheng Su https://orcid.org/0000-0001-6514-3596

References

[1] Kojima A, Teshima K, Shirai Y and Miyasaka T 2009 *J. Am. Chem. Soc.* **131** 6050
[2] Stranks S D and Snaith H J 2015 *Nat. Nanotech.* **10** 391
[3] Jiang Q, Zhao Y, Zhang X, Yang X, Chen Y, Chu Z, Ye Q, Li X, Yin Z and You J 2019 *Nat. Photon.* **13** 460
[4] Cao Y *et al* 2018 *Nature* **562** 249
[5] Lin K *et al* 2018 *Nature* **526** 245
[6] Liu K, Chen S, Wu J, Zhang H, Qin M, Lu X, Tu Y, Meng Q and Zhan X 2018 *Energy Environ. Sci.* **11** 3463
[7] Hu X, Zhang X D, Liang L, Bao J, Li S, Yang W L and Xie Y 2014 *Adv. Funct. Mater* **24** 7373
[8] Dou L T, Yang Y, You J B, Hong Z R, Chang W H, Li G and Yang Y 2014 *Nat. Commun.* **5** 5404
[9] Dong R, Fang Y, Chae J, Dai J, Xiao Z, Dong Q, Yuan Y, Centrone A, Zeng X C and Huang J 2015 *Adv. Mater.* **27** 1912
[10] Ahmadi M, Wu T and Hu B 2017 *Adv. Mater.* **29** 1605242
[11] Dong Y, Zou Y, Song J, Song X and Zeng H 2017 *J. Mater. Chem.* C **5** 11369
[12] Wangyang P, Gong C, Rao G, Hu K, Wang X, Yan C, Dai L, Wu C and Xiong J 2018 *Adv. Opt. Mater.* **6** 1701302
[13] Miao J and Zhang F 2019 *J. Mater. Chem.* C **7** 1741
[14] Wang Y *et al* 2017 *Org. Electron.* **49** 355
[15] Lee Y, Kwon J, Hwang E, Ra C H, Yoo W J, Ahn J H, Park J H and Cho J H 2015 *Adv. Mater.* **27** 41
[16] Chen S, Teng C, Zhang M, Li Y, Xie D and Shi G 2016 *Adv. Mater.* **28** 5969
[17] Gu L and Fan Z 2017 *Light: Sci Appl.* **6** e17090
[18] Huang F, Peng Y and Liu G 2019 *J. Phys. Chem.* C **123** 11073
[19] Xia H R, Li J, Sun W T and Peng L M 2014 *Chem. Commun.* **50** 13695
[20] Chen H Y, Bian W P, Wang Y F, Yan J, Li L, Wang H B and Li B S 2019 *Chin. J. Lumin.* **40** 1261
[21] Hu W, Cong H, Huang W, Huang Y, Chen L, Pan A and Xue C 2019 *Light: Sci Appl.* **8** 106
[22] Shen K *et al* 2019 *J. Mater. Chem.* A **7** 6134
[23] Teng C J, Xie D, Sun M X, Chen S, Yang P and Sun Y L 2016 *ACS Appl. Mater. Interfaces* **8** 31289
[24] Cao F, Tian W, Meng L, Wang M and Li L 2019 *Adv. Funct. Mater.* **29** 1808415
[25] Xua H, Tong S, Zhang C, Wang C, Sun J, He J, Zhang J, Gao Y and Yang J 2018 *Appl. Phys. Lett.* **112** 233301
[26] Qin L, Wu L, Kattel B, Li C, Zhang Y, Hou Y, Wu J and Chan W L 2016 *Adv. Funct. Mater.* **27** 1704173
[27] Liu Y, Jia R, Wang Y, Hu Z, Zhang Y, Pang T, Zhu Y and Luan S 2017 *ACS Appl. Mater. Interfaces* **9** 15638
[28] Shen Y, Yu D, Wang X, Hou C, Wu Y, Zhu Z and Zeng H 2018 *Nanotechnology* **29** 085201
[29] Wang Y, Zhang T, Zhang P, Liu D, Ji L, Chen H, Chen Z D, Wu J and Li S 2018 *Org. Electron.* **57** 263
[30] Tian Y, Xue H, Tang F, Wang L and Jiang H 2019 *Mater. Res. Express* **6** 116219
[31] Xu J *et al* 2015 *Nat. Commun.* **6** 7081
[32] Liu C, Wang K, Du P, Chao Y, Meng T and Gong X 2015 *Adv. Energy Mater.* **5** 1402024
[33] Chiang C H and Wu C G 2016 *Nat. Photon.* **10** 196
[34] Fang Y, Bi C, Wang D and Huang J 2018 *ACS Energy Lett.* **2** 782
[35] Wu H, Su Z, Jin F, Zhao H, Li W and Chu B 2018 *Org. Electron.* **57** 206
[36] Hou F, Su Z, Jin F, Yan X, Wang L, Zhao H, Zhu J, Chu B and Li W 2015 *Nanoscale* **7** 9427